Available online at www.sciencedirect.com
SCIENCE DIRECT
Polymer 46 (2005) 6736–6745
polymer
www.elsevier.com/locate/polymer

Direct fluorination of poly(*p*-phenylene)

M. Dubois[a,*], K. Guérin[a], J. Giraudet[a], J.-F. Pilichowski[b], P. Thomas[c], K. Delbé[c], J.-L. Mansot[c], A. Hamwi[a]

[a]*Laboratoire des Matériaux Inorganiques, UMR CNRS-6002, Université Blaise Pascal Clermont-Ferrand, 63177 Aubière, France*
[b]*Laboratoire de Photochimie Moléculaire et Macromoléculaire, UMR CNRS-6505, Université Blaise Pascal Clermont-Ferrand, 63177 Aubière, France*
[c]*Groupe de Technologie des Surfaces et Interfaces, EA CNRS-2432, Faculté des Sciences Exactes et Naturelles, Université des Antilles et de la Guyane, 97159 Pointe À Pitre Cedex, France*

Received 5 April 2005; received in revised form 15 June 2005; accepted 15 June 2005
Available online 19 July 2005

Abstract

Because of its good chemical and thermal stability due to the π-delocalization along the polymer chain, poly(*p*-phenylene) was used as starting material for fluorination to obtain new carbon fluoride. A complete characterization of both the virgin polymer, in order to define parameters such as the chain length and the degree of crystallinity, and the fluorinated materials was performed by complementary techniques (^{19}F, ^{1}H and ^{13}C NMR, XRD, FT-IR and EPR). From these data, possible fluorination mechanisms are discussed. Finally, tribological properties have been also studied for the fluorinated samples and compared to those of conventional graphite fluorides.

Keywords: Polymer chemistry; Polymer physical chemistry

1. Introduction

Fluorination is known to be one of the most effective chemical methods to modify, and therefore, to control the physicochemical properties of carbon materials [1,2]. The variety of starting carbonaceous materials is wide including graphite [1,3], nanotubes [4,5], fibers [6,7], fullerenes [8–10], diamond-like carbons [11], polymers [12–14],…

Potential applications of these fluorinated materials are various such as positive electrode in high energy density lithium batteries [15], solid lubricants [16,17], gas storage, fluorination releasing agents, water or oil repellents, and so on [1,2,16,18]. Therefore, these fluorinated carbons have been the focus of a great number of studies. The structural properties of the starting carbon materials strongly influence both the fluorination level and the physicochemical properties of resulting compounds. In particular, the C–F bond nature differs as a function of the starting materials and of the fluorination process, as exemplified by the case of graphite fluorides: on one hand, when the fluorination of graphite is performed at 350 and 600 °C, graphite fluorides $(C_2F)_n$ and $(CF)_n$, respectively, are obtained [18]. These latter are electronic insulators and the C–F bond is covalent involving a sp^3 hybridization of the carbon atom. On the other hand, conducting fluorine–graphite intercalation compounds (fluorine-GICs, C_xF) and semi-ionic graphite fluorides are obtained at temperatures below 100 °C using either a gaseous mixture of fluorine with HF or volatile fluorides MF_y (BF_3, IF_5, IF_7, WF_6, …) [1,19] or F_2, HF and MF_y mixture [20–22]. In these cases, the nature of the C–F bond evolves from ionic for low fluorine content to semi-ionic for higher fluorine content (carbon atoms in such compounds are mainly sp^2 hybridized).

Most of these fluorinated materials exhibit a two-dimensional lamellar structure. The goal of the present work is to study the fluorination of a linear π-electron conjugated system. The electronic properties of such systems are also of great interest. A conjugated polymer, poly(*p*-phenylene) abbreviated as PPP, has then been used as starting materials for fluorination. It consists of benzene rings linked exclusively in para position. This polymer exhibits good chemical and thermal stability, up to 500 °C, due to π-delocalization along the polymer chain. Amongst the various synthesis of PPP, chemical [23–27] or

* Corresponding author. Tel.: +33 4 73 40 71 05; fax: +33 4 73 40 71 08.
E-mail address: marc.dubois@univ-bpclermont.fr (M. Dubois).

0032-3861/$ - see front matter © 2005 Elsevier Ltd. All rights reserved.
doi:10.1016/j.polymer.2005.06.029

electrochemical [28], chemical Kovacic's method [26] has been chosen because it allows long chains to be formed, longer than 12 phenyl rings per chain, whereas Yamamoto [23] and Taylor [25] synthesis result in chains with 9 phenyl units length [27,29]. The electrochemical method of Fauvarque results also in long chains (12 phenyl rings per chain) but in lower crystallinity than Kovacic PPP. A wide fluorine range could be obtained as a function of fluorination conditions, i.e. temperature and duration; a maximal composition of $(C_6F_{10})_n$ could be theoretically obtained.

As demonstrated by several authors [2,30], nuclear magnetic resonance studies are well adapted to fluorocarbons characterization because they can give information about both the carbon hybridization and carbon–fluorine interaction, i.e. the nature of the C–F bond. Solid state NMR correlated with X-ray diffraction, Fourier transform infrared (FT-IR) and electron paramagnetic resonance (EPR) spectroscopies, are necessary to understand the fluorination processes and to investigate the maintaining of the phenyl ring within the polymer chain.

Tribological experiments have also been performed in order to evaluate the friction properties of fluorinated PPP. Indeed, if the good lubricating performances of main conventional solid lubricants are due to their bidimensional lamellar structure, there is few data in the literature concerning the tribological applications of 1D materials. So the friction properties of fluorinated PPP will be compared to those of conventional high temperature graphite fluoride.

2. Experimental

Poly(*p*-phenylene) was synthesized according to the Kovacic's method [26] which consists in a cationic polymerization of benzene with $AlCl_3$ and $CuCl_2$. The brown insoluble powder was washed out with hot hydrochloric acid to remove the catalyst residues and then heated at 400 °C under vacuum for further purification. The fluorination treatment of PPP was performed as follow: the virgin PPP (200 mg) was heated at 150 °C for half an hour in a dry nitrogen atmosphere to remove traces of water molecules adsorbed during exposure to air atmosphere; after cooling, it was then placed at room temperature or heated at 100 °C for various duration (4, 5, 12, 24 h) in pure F_2 atmosphere (Solvay Fluor and Derivate, purity 98–99% (V/V) with HF max. 0.5% (V/V) and other gases, primarily O_2/N_2 at approximately 1.0% (V/V)). The pressure of fluorine gas used in fluorination experiments was fixed at 1 atm. As the temperature of fluorination reaction is abbreviated as T_F, the samples are named PPPF (T_F-4 h), PPPF (T_F-5 h), PPPF (T_F-12 h) and PPPF (T_F-24h) with T_F equal to 25 and 100 °C. The composition was determined both by weight uptake and chemical analysis.

Powder X-ray diffraction (XRD) measurements were carried out using a Siemens D501 diffractometer working with a Cu K_α radiation. Fourier transform infrared spectroscopy (FT-IR) was performed using spectrometer SHIMADZU FT-IR-8300; the spectra were recorded by transmission in a dry air atmosphere between 400 and 4000 cm^{-1} with 20 spectra accumulation through a pellet (2 mg of the sample material diluted in 200 mg of KBr).

Static ^{19}F NMR experiments were carried out at room temperature on a Bruker AVANCE DSX 300 spectrometer at 282.38 MHz. The external reference was CF_3COOH; all the chemical shifts are referenced with respect to $CFCl_3$ ($\delta_{CF_3COOH} = -78.5$ ppm vs $CFCl_3$). Magic angle spinning (MAS) ^1H NMR and ^{13}C NMR spectra were recorded at room temperature (spectrometer operating at 300.13 and 75.47 MHz, respectively) and were performed with a spinning speed of 4 and 10 kHz with Bruker 4 mm MAS probe. ^1H chemical shifts are referred to tetramethylsilane (TMS) by using adamantane as an external standard (+1.74 ppm from TMS). ^{13}C chemical shifts are given with respect to resonance of TMS. A simple sequence ($\pi/2$-acquisition) was used with a single pulse duration equal to 5.00, 8.25 and 2.75 μs for ^1H, ^{13}C and ^{19}F NMR measurements, respectively. The recycling time $D1$ were equal to 6, 25 and 2 s for ^1H, ^{13}C and ^{19}F NMR, respectively.

EPR spectra were recorded using a X Band Bruker EMX spectrometer equipped with a standard variable temperature accessory and operating at 9.653 GHz. Diphenylpicrylhydrazyl (DPPH) was used to calibrate the resonance frequency ($g = 2.0036 \pm 0.0002$) and the densities of spin carriers D_s (D_s is the number of unpaired electronic spins per gram of carbon). Spectra acquisition were carried out at 6.35 mW microwave power, with modulation amplitude of 2 G and with 100 kHz frequency modulation in order to avoid saturation and line shape distortions. Bruker WINEPR and WinSimfonia were used for spectra processing and simulations, respectively.

The tribological properties of the compounds were evaluated using a ball-on-disc tribometer consisting of an AISI 52100 steel ball rubbing against the AISI 52100 steel disc of 10×2 mm dimensions covered with a film of studied lubricant. Before deposit procedure, discs were polished with 1000 and 400 μm abrasive paper and cleaned in ethanol and acetone ultrasonic baths to completely remove impurities and abrasive particles. The final peak to peak roughness of the disc before film deposits was measured to 200 nm. This final roughness is needed to fix the solid lubricant film on the friction surfaces. The lubricant film is deposited by the burnishing technique. The tribological tests were performed under a normal load of 10 N and a sliding speed of 2 mm s^{-1}. The friction coefficient μ, defined as the ratio of lateral force on normal load, was measured with a computer-based data acquisition system.

3. Results and discussion

First, experimental conditions of preparation and

compositions of the resulting fluorinated materials are displayed in Table 1.

3.1. Solid state NMR

In order to investigate the fluorination efficiency of poly(*p*-phenylene), a careful characterization of the virgin polymer is necessary, giving parameters such as the degree of crystallinity and the chain length of the polymer. This latter can be evaluated from ^{13}C NMR data. The spectrum of virgin PPP was recorded with magic angle procedure operating with a spinning rate of 4 kHz, contrary to the other samples for which 10 kHz was applied (Fig. 1). The surface ratio of the lines centered at +128 and +139 ppm allows the chain length to be evaluated. As a matter of fact, these lines are assigned to carbon atoms bound to hydrogen atoms (with surface S_{C-H}) and carbon atoms linking the phenyl rings (S_{C-C}), i.e. non-hydrogenated, respectively [27,31,32]. S_{C-H}/S_{C-C} is equal to 2.19. Neglecting the possible substitution at chain edges of hydrogen by chlorine atoms resulting from the synthesis, this value corresponds to a chain length of 15–16 phenyl rings per chain.

For the sample fluorinated at 25 °C for 5 h (PPPF (25 °C-5 h)), the intensity of the C–H line ($\delta \approx +128$ ppm) decreases significantly contrary to the one at +139 ppm (C–C) indicating that a part of the phenyl rings is conserved during the first stage of fluorination. Depending of the interaction of carbon with fluorine atoms, the chemical shift of sp^2 type carbon varies from +120 ppm in pure graphite [2,30] to +128 and +137 ppm in semi-ionic graphite fluoride prepared at room temperature using a HF–BF_3 mixture [33] and a HF–IF_5 one [22,34], respectively; in these latter materials, sp^2 carbon hybridization is still maintained allowing the planarity of the graphene sheets to be conserved. By analogy, the weak peak at +160 ppm could result from interaction of carbon atoms of the maintained phenyl rings with fluorine; this interaction results in the shift of the NMR line from +139 to +160 ppm. This line disappears when the fluorination duration increases (24 h at room temperature). Moreover, the NMR spectrum of PPPF (25 °C-5 h) shows a broad signal composed of several contributions showing the complexity of this material and its structural disorder.

Whatever the fluorinated sample, ^{13}C MAS-NMR spectra exhibit two lines located at +88 and +110 ppm

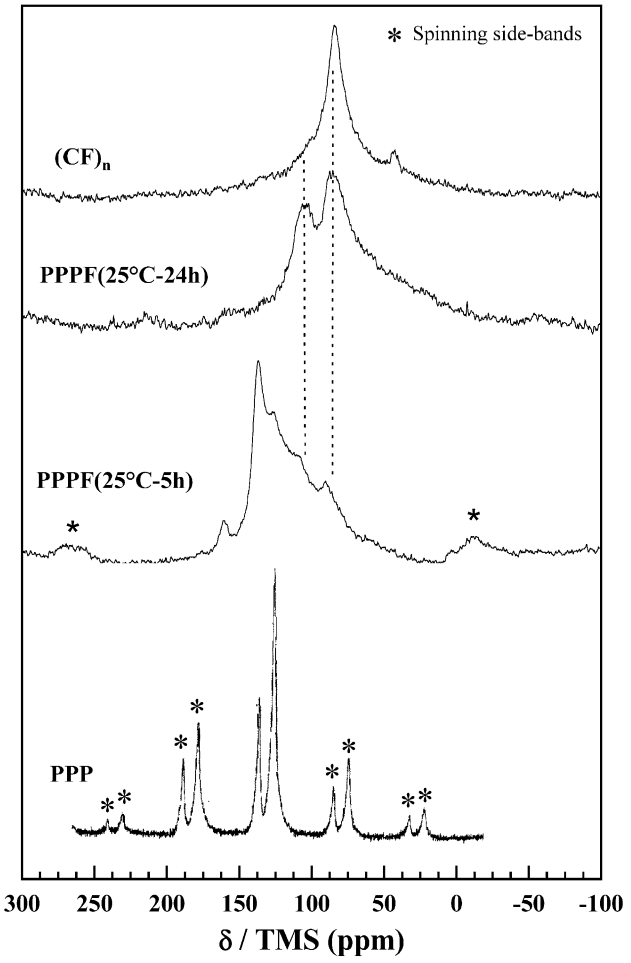

Fig. 1. ^{13}C MAS-NMR spectra of virgin poly(*p*-phenylene) and polymer treated during various fluorination time compared to high graphite fluoride (CF_n).

(Fig. 1). For PPPF (25 °C-5 h), only shoulders are present. According to the literature about fluorinated carbons such as graphite fluorides [2,30,35–38], fluorinated charcoal and fluorinated coronene [39], these lines are characteristic of carbon atoms involved in covalent C–F bonds (fluorocarbon rigid matrix in graphite fluoride) and of CF_2 groups localized either at the sheets edges of the fluorographite layers (and/or in other defected structures) or along fluorinated polymer chains. Characteristic chemical shifts are displayed in Table 2. For comparison, graphite fluoride $(CF)_n$ obtained by direct fluorination of graphite at 600 °C

Table 1
Experimental conditions of fluorination

Sample	Fluorination temperature (°C)	Duration (h)	Formulation
PPP	–	–	$C_6H_{3.81}$ [a]
PPPF (25 °C-5 h)	25	5	$C_6F_{5.9}$ [b]
PPPF (25 °C-12 h)	25	12	$C_6F_{7.6}$ [b]
PPPF (25 °C-24 h)	25	24	$C_6F_{8.0}$ [b] ($C_6F_{8.25}H_{1.75}$)[a]
PPPF (100 °C-4 h)	100	4	$C_6F_{6.8}$ [b] ($C_6F_{8.95}H_{1.13}$)[a]

[a] Evaluated from chemical analysis.
[b] Evaluated from weigth uptake results.

consists mainly of covalent C–F bonds (resulting in a strong line at +84 ppm on the NMR spectrum) and small amount of CF_2 groups localized at the sheets edges (+110 ppm).

Fig. 2 displays the evolution of room temperature ^{19}F NMR spectra of fluorinated poly(*p*-phenylene) as a function of the temperature (T_F) and the duration of fluorination. For the samples treated at room temperature for 5 and 12 h, the spectra exhibit at least three broad resonances centered near −75, −125 and −195 ppm; this latter results from the rigid fluorinated carbon lattice because this resonance is typical of mainly covalent C–F bonds in fluorinated graphite compounds (Table 2) [2,21,22,30,34,38,39]. The two first lines at −75 and −125 ppm are assigned to CF_3 and CF_2 groups [38,39], respectively.

The spectrum of PPPF (25 °C-5 h) exhibits a line shape with a rectangular envelope typical of dipolar coupling among the fluorine atoms in the fluorocarbon matrix. Such a contribution is reported for covalent graphite fluorides $(CF)_n$ and $(C_2F)_n$ [30,35] and for some inorganic fluorides, e.g. LiF and CaF_2 in naphthalene [40].

When the time or the temperature of fluorination increases, two peaks, centered at −70 and −230 ppm, are well separated; the evolution of their intensities is opposite when T_F increases. By analogy with various fluorinated organic molecules and fluoropolymers [41], the line at −70 ppm, which is more intense for T_F equal to 100 °C, is assigned to CF_3 groups whereas the one at −230 ppm is attributed to C–F bonds; contributions of CF_2 and CHF groups are also possible. The presence of the strong lines of CF_3 groups and its evolution with increasing time and temperature of fluorination indicate the opening of some fluorocarbon rings during fluorination resulting in the formation of $–CF_3$, $–CF_2–CF_3$, $–CF_2–CF_2–CF_{3,\ldots}$ grafted to remaining fluorocarbon rings. Such a linear configuration reduces the dipolar coupling between fluorine nuclei leading to a better resolution of the two main bands in the NMR

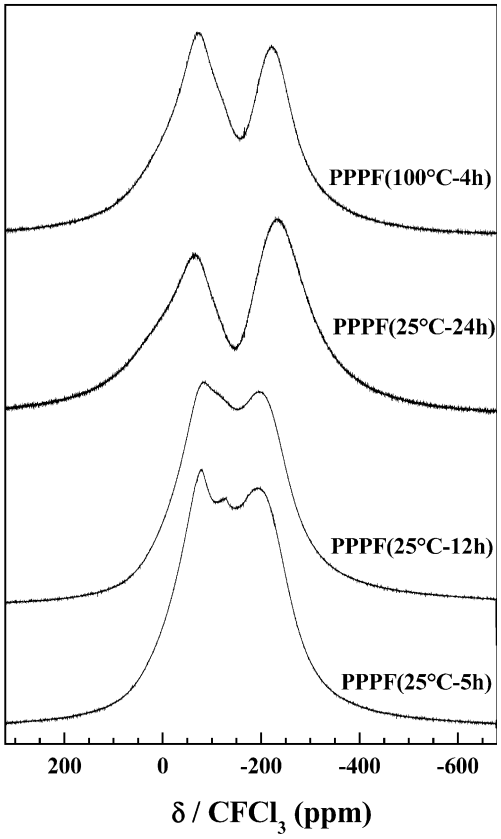

Fig. 2. ^{19}F NMR spectra at room temperature of PPP treated under F_2 at 25 and 100 °C for various duration.

spectra in comparison with PPPF (25 °C-5 h) and PPPF (25 °C-12 h). The presence of hydrogenated groups in the resulting samples is confirmed by both chemical analysis (Table 1) and ^1H MAS-NMR. Indeed, for these latter experiments, in the case of the polymer fluorinated at room temperature for 5 and 24 h (Fig. 3), the spectra exhibit a strong resonance at +9 ppm (vs TMS). This latter decreases

Table 2
NMR chemical shifts of fluorinated carbon materials

Samples	NMR chemical shifts						
	^{13}C/TMS				$^{19}F/CFCl_3$		
	C	C^{α}	C–F	CF_2	C–F	CF_2	CF_3
Graphite [2,30]	120						
Covalent (CF_n) [2,32,36–38]			84–88	110	−170 to −190	−110	
Semi-ionic C_xF							
$CF_{0.89}(IF_y)_x(HF)_z$ [21,22,34]		134	79		−140 to −160		
$CF_{0.47}(BF_4)_x(HF)_z$ [33]		125	79		−140 to −160		
Fluorinated charcoal [39]		129	86	112	−140 to −200	−100 to −150	−50 to −90
Fluorinated coronene [39]		136	86	113			
PVDF $(CF_2CH_2)_n$ [41]				120		−115 (our data)	
a							−75.1
b						−118.1	
c					−183.7		
PPPF (25 °C-5 h)	138	160	84	110	−195	−125	−75
PPPF (25 °C-24 h)			84	110	−230		−70

α Carbon atoms in weak interaction with fluorine. a: $–CF_2–CF_2–CF(CF_3*)–CH_2–CF_2–$; b: $–CH_2–CF_2–CF_2*–CF(CF_3)–CH_2–$; c: $–CF_2–CF_2–CF*(CF_3)–CH_2–CF_2–$; where asterisk indicates the fluorine atom concerned.

in intensity when the fluorination time increases indicating a conversion of C–H bonds into C–F ones. A shoulder near +5 ppm is also observed and is assigned to low amounts of water molecules absorbed on the carbonaceous surface; its observation suggests that the total amount of ^{1}H nuclei (from fluorinated PPP and H_2O) is very low in PPPF (25 °C-24 h).

The comparison with fluorinated coronene ($C_{24}H_{12}$) is interesting; the fluorination of this compound is achieved at room temperature, i.e. 23 °C using firstly a diluted F_2/He mixture and then neat fluorine to ensure complete reaction. The product consisted of a mixture of perfluorocoronene ($C_{24}F_{36}$) and a second fluorocarbon ($C_{24}F_{30}$) in which the π-character of one phenyl ring per molecule is maintained in the structure [39] indicating that the fluorination is not complete as in the case of fluorinated PPP.

From ^{13}C, ^{19}F and ^{1}H NMR data, it is concluded that the fluorination occurs with successive steps, firstly, for low duration, on one hand a part of the unsaturated phenyl rings are maintained, on the other hand, CF_2 groups are formed resulting in a cyclohexane-like armchair (or boat) conformation of the fluorinated rings of idealized formula (–C_6F_{10}–). Then, some of these rings are broken to form short aliphatic fluorinated oligomers. These hypotheses will be discussed as a function of the FT-IR characterization in Section 3.2.

3.2. FT-IR and XRD characterizations

Infrared spectroscopy data can also provide an estimation of the chain length either by comparing the ratio of the main band intensities (Fig. 4 and Table 3) I_{805}/I_{764} or $I_{805}/(I_{764}+I_{697})$ to those of phenylene oligomers [26,42] or by the formula $(2(I_{805}/I_{697})+2)$ [43]. From the three methods, the obtained value is about 15–16 phenyl units per chain of PPP in accordance with NMR data. The discrepancy between the formulation of virgin PPP ($C_6H_{3.81}$) and the idealized formula $(C_6H_5)[(C_6H_4)_{14}](C_6H_5)$, i.e. ($C_6H_{4.125}$), is related to the defects in the polymer such as crosslinking and residual catalyst species. As a matter of fact, the virgin polymer also contains small amounts of oxygen (mass percentage 0.4% obtained vs chemical analysis) and residual catalyst residues: Cl (1.1%), Al (0.4%) and Cu (0.1%). Chlorine atoms are probably located on the chain edges and replace hydrogen atoms.

On one hand, after the fluorination for 5 h at room temperature, a quasi-total disappearance of the vibration peaks of PPP in the range 697–860 cm^{-1} is noted. These ones are related to C–C and C–H vibrations of mono-substituted and parasubstituted phenyl rings (Table 3), this confirms the conversion of C–H bonds into C–F ones in accordance with the appearance of the strong band at 1220 cm^{-1}, assigned to covalent C–F [19]. On the other hand, the strong bands at 1480, 1398 and 1000 cm^{-1}, which are characteristic of the C–C vibrations of paradisubstituted phenyls, broaden and shift towards the lower wavenumbers by about 20 cm^{-1} indicating the maintain of a part of the phenyl rings as observed from ^{13}C NMR data. An intense band centered near 1220 cm^{-1} appears after the fluorination and increases in intensity with the fluorination time at room temperature. This strong band is assigned to covalent C–F bonds in fluorinated carbons in particular in conventional graphite fluoride $(CF)_n$ [19]; its broad shape results from superimposition of several contributions, i.e. CF_3, CF_2, CF groups.

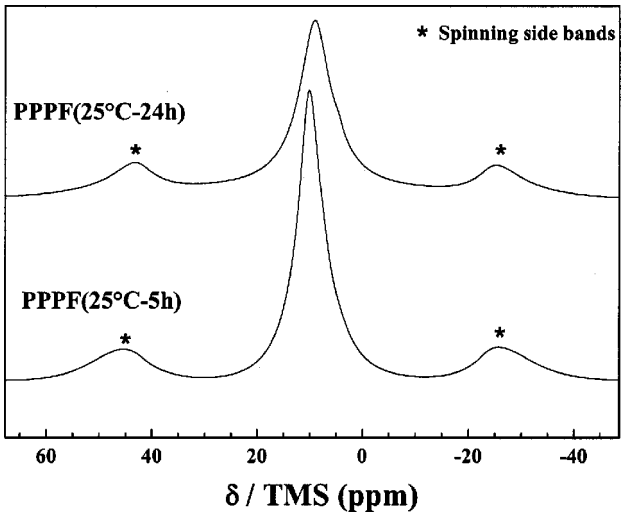

Fig. 3. ^{1}H MAS-NMR spectra of fluorinated poly(*p*-phenylene): PPPF (25 °C-5 h) and PPPF (25 °C-24 h).

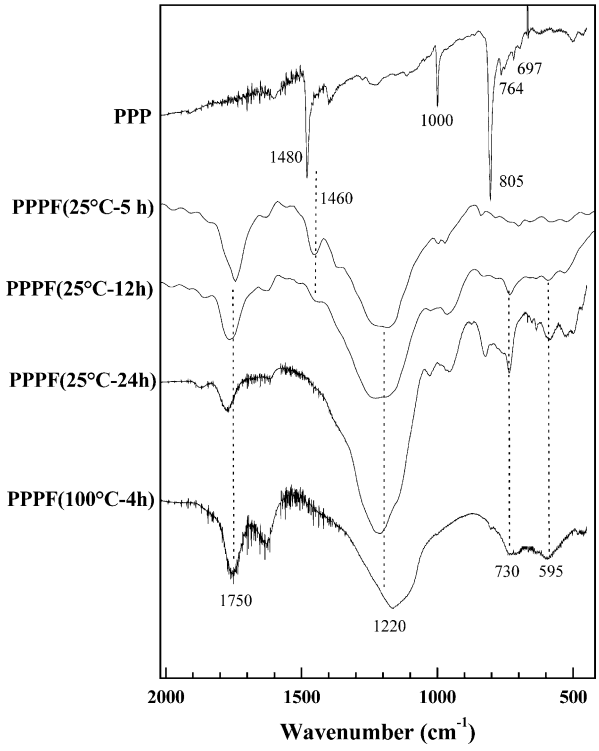

Fig. 4. FT-IR spectra of PPP and polymer fluorinated as a function of the fluorination conditions.

Table 3
Assignment of the vibration modes

Wavenumber (cm^{-1})	Vibration mode
697, 764	Out-of-plane C–H vibration (δ_{C-H}) of monosubstituted phenyl rings
805	Out-of-plane C–C vibration (δ_{C-C}) of parasubstituted phenyl rings
860	Out-of-plane C–H vibration (δ_{C-H}) of an isolated hydrogen
1000, 1398 and 1480	In-plane C–C vibration (ν_{C-C}) of parasubstituted phenyl rings
~3000	C–H vibration of aromatic rings (ν_{C-H})
1220	Vibration of covalent C–F bonds
1750	C=O vibration
730	CF_3 and CF_2 symmetric deformation [43,44]
595	CF_3 and CF_2 antisymmetric deformation [43,44]

For the samples obtained with longer fluorination time or at 100 °C, two broad bands near 720 and 600 cm^{-1} magnify the possible presence of short fluorinated aliphatic chains, which are branched on the fluorinated polymer.

A band at about 1750 cm^{-1} is observed whatever the fluorination conditions, it may be related to C=O vibration in accordance with previous works about the direct fluorination of commercial polymers [14,44–49]. Such C=O group can be formed during the exposure of the materials in air atmosphere after the treatment. The use of pure fluorine gas prevents the formation of these oxygenated groups during the fluorination process. The materials obtained from fluorination are inhomogeneous containing several conformational defects in comparison with idealized $(C_6F_{10})_n$ chains which are constituted of linked fluorinated armchair rings.

Fig. 5 displays the XRD patterns of PPP and fluorinated samples. A degree of crystallinity close to 30% was determined for the virgin polymer using both the methods of Ruland [50] and Hermans [51]. The four main diffraction peaks of the virgin polymer centered at 2θ equal to 19.6° (d=4.53 Å), 22.6° (d=3.94 Å), 27.5° (d=3.24 Å), and 43.0° (d=2.10 Å), are indexed, respectively, as (110), (200), (210) and (002) reflections in monoclinic system (space group $P2_1/c$) [52]. These ones disappear totally after fluorination for 5 and 12 h at room temperature. The materials are then amorphous. On the contrary, when the time or the temperature of fluorination increases, a low crystalline order appears as magnified by two well defined diffraction lines, at 14.3° ($d \approx 6.19$ Å) and 40.6° ($d \approx 2.22$ Å). Surprisingly, the XRD patterns PPPF (25 °C-24 h) and PPPF (100 °C-4 h) are close to that of graphite fluoride $(CF)_n$. For this latter, the main reflection lines at 14.4° ($d_i \approx 6.16$ Å) and 40.8° ($d \approx 2.21$ Å) were assigned to 001 reflection (corresponding to the average interlayer spacing) and to 100 reflection of in-plane graphite network, respectively. We believe that, in an idealized view, the fluorinated chains constituted of linked ($-C_6F_{10}-$) rings are organized in order to minimize the fluorine atoms repulsion, i.e. the stacking of the chains; this simulates the arrangement occurring in conventional high temperature graphite fluoride (Fig. 6).

For $(CF)_n$, the C–C in-plane length can be calculated from the diffraction reflection at 40.7° which is assigned to 100 reflection of in-plane graphite network (hexagonal system) with corresponding reticular distances d_{100}= 2.22 Å ($d_{C-C}=(2/3)d_{100}$ and the a hexagonal parameter is given by the relation $a = d_{100}(2/\sqrt{3})$). So, the C–C length (or its projection) is equal to 1.48 Å in $(CF)_n$; such a value is close to that occurring when the carbon atoms exhibit a pure sp^3 character (1.54 Å in diamond). Assuming that the structure of fluorinated PPP is similar to that of $(CF)_n$, the same calculation provides C–C distance close to 1.48 Å for highly fluorinated polymer showing that the carbon hybridization changes from sp^2 character for PPP to sp^3

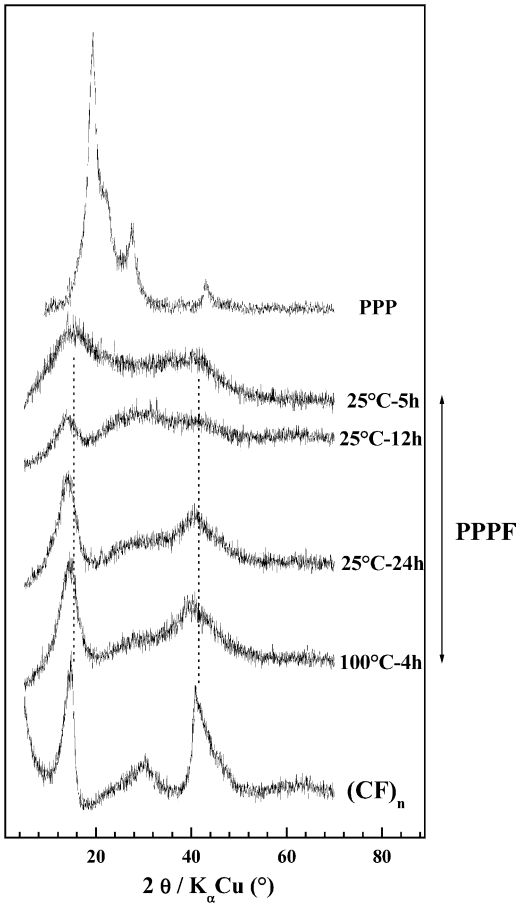

Fig. 5. X-ray diffractograms of poly(*p*-phenylene) and fluorinated samples.

one for the fluorinated PPP. The molecular geometry of the virgin PPP is planar with in-ring C–C bond distances of 1.41 Å and a C–C distance between phenyl rings equal to 1.45 Å.

3.3. EPR data

The EPR spectrum of the virgin PPP is symmetrical and consists of a single Lorentzian line (Fig. 7). The peak-to-peak linewidth ΔH_{pp} and the g-value are equal to 5.2 ± 0.2 G and 2.0029 ± 0.0005, respectively; these values are in accordance with those reported by many authors [27]. EPR lines are assigned either to connection defects of the phenyl rings, i.e. crosslinking or to residual radicals resulting from the synthesis which are trapped in the polymer bulk and then sterically inaccessible to air atmosphere. The spin density of the virgin polymer (i.e. the spins number per gram noted D_s) is close to 1.7×10^{17} spin g^{-1}.

The EPR spectra at room temperature change significantly after the fluorination (Fig. 7 and Table 4) except for the g values which stay close to 2.0030 ± 0.0005 whatever the sample, this g-factor being typical of free radicals and/or localized structural defects.

After the treatment at room temperature for 5 h, two new signals appear: one broad line with a linewidth close to 90 G and a narrow line ($\Delta H_{pp} \approx 8$ G). The origin of the broad line was identified as carbon dangling bonds having a localized spin. Such spin carriers have been proposed for other fluorinated graphite obtained in F_2 atmosphere in the 350–600 °C reaction temperature range [22,35], in fluorinated nanosized graphite fluorides [53] and in fluorinated amorphous carbon thin film [54,55]. Contrary to the narrow line, which is a single signal, the broad EPR line cannot be simulated by a pure Lorentzian or Gaussian profile. The broad shape could result from a non-resolved super-hyperfine structure (SHFS) of the dangling bond electrons interacting with the neighboring fluorine nuclei [22,35]. Dangling bond centers could adopt different configurations of surrounding fluorine atoms; this disorder leads to the non-solved hyperfine structure.

The narrow signal ($\Delta H_{pp} \approx 8$ G) could be assigned to radicals of residual polymer inaccessible to fluorine or to a different kind of dangling bonds (defects with a different environment). On the basis of NMR and FT-IR data, the second hypothesis is more probable because of the quasi-disappearance of the lines typical of the polymer after

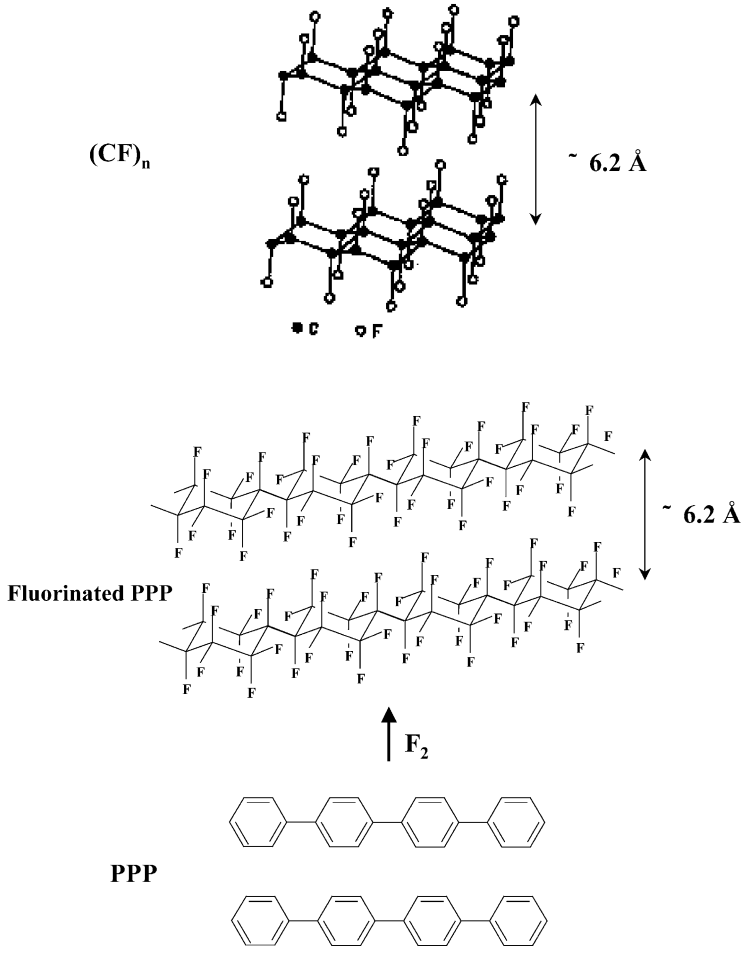

Fig. 6. Comparison of fluorinated PPP and graphite fluoride structures.

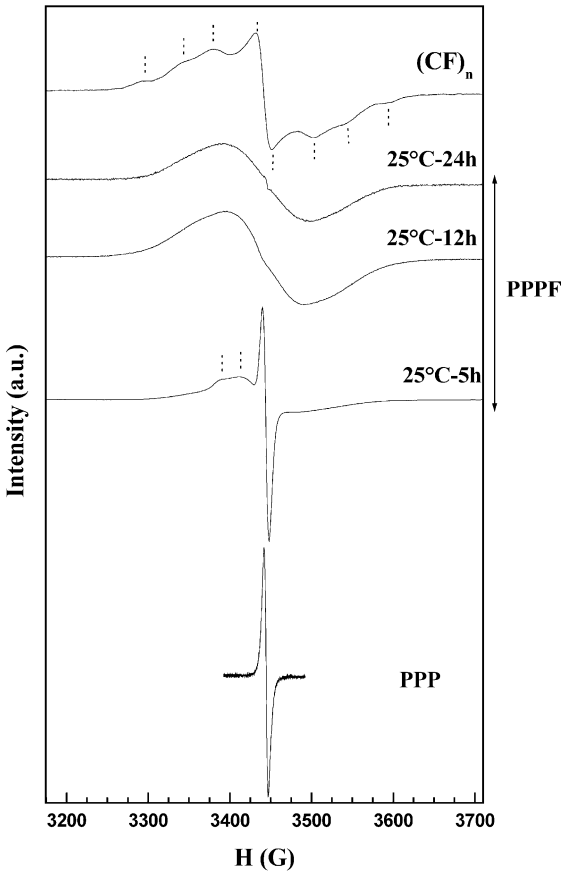

Fig. 7. EPR spectra of the fluorinated samples and the virgin polymer at room temperature compared to conventional graphite fluoride $(CF)_n$.

fluorination even for short duration at room temperature. Two types of dangling bonds also coexist in high temperature graphite fluoride: a narrow line is present on the EPR spectrum of this material ($\Delta H_{pp} = 20 \pm 1$ G) in addition to the hyperfine line related to interaction between dangling bond electron and six neighboring fluorine nuclei (nuclear spin $I = 1/2$) resulting in the splitting of the EPR spectrum into seven lines ($(2nI+1)=7$). The simulation of these signals leads to the hyperfine parameter $A = 45 \pm 2$ G, a linewidth $\Delta H_{pp} = 36 \pm 2$ G and $g = 2.003 \pm 0.001$ [34]. Moreover, the formation of peroxy $RO_2^{\cdot}$ radicals superimposed with dangling bonds can not be excluded.

It must be noted that in the case of PPPF (25 °C-5 h), the EPR line is more complicated with a possible hyperfine structure (marked with dashed lines on Fig. 7), which is not enough resolved to be simulated; nevertheless, the hyperfine parameter and the number of neighboring fluorine nuclei seems to be lower than for $(CF)_n$. On the contrary, for PPP fluorinated at room temperature for 12 and 24 h, the linewidth of the line envelop is close to that of graphite fluoride ($\Delta H_{pp} \approx 100$ G) indicating close hyperfine parameters. On the other hand, higher disorder for the fluorinated polymer in comparison with $(CF)_n$ results in the non-solved SHFS. So, this indicates similar configuration of the neighboring fluorine nuclei around the dangling bonds as suggested from XRD data.

The formation of dangling bonds, i.e. conformational defects during fluorination results in a significant increase of the spin density D_s for fluorination durations of 5 and 12 h (Table 4). For the longer fluorination time (24 h) at room temperature, a slight decrease of D_s is then observed. After the fluorination, the samples were exposed to air atmosphere and then investigated; as their EPR spectra did then not change as a function of the exposure time in air, the electronic spin carriers, which are formed upon fluorination and partially converted in air atmosphere, are stable in these conditions.

3.4. Tribological performances

The tribological behaviour of various samples of PPPF and conventional $(CF)_n$ as reference were investigated under air and under argon. The results are summarized in Figs. 8 and 9. As it can be seen, the friction coefficients recorded for all samples remain stable during the friction tests, pointing out the good stability and durability of the PPPF films. Either under air or under argon, friction coefficients recorded for PPPF samples are higher than commercial $(CF)_n$ ones. Whereas friction coefficient of $(CF)_n$ remains unchanged as a function of atmosphere, the friction properties of PPPFs appear better under argon than under air ($\mu_{PPPF\ (25\ °C\text{-}5\ h)} = 0.18$ and $\mu_{PPPF\ (25\ °C\text{-}24\ h)} = \mu_{PPPF\ (100\ °C\text{-}4\ h)} = 0.16$ under air compared to $\mu_{PPPF\ (25\ °C\text{-}5\ h)} = 0.16$ and $\mu_{PPPF\ (25\ °C\text{-}24\ h)} = \mu_{PPPF\ (100\ °C\text{-}4\ h)} = 0.13$ under argon). It shows that PPPF tribological properties are significantly affected by environmental conditions (especially presence of water vapour or oxygen). This atmosphere dependant behaviour of the PPPF compounds can be attributed to the presence in their structure of C–H bonds subjected to enhance the hydrophilic properties of fluorinated PPP compared to perfluorinated materials ($(CF)_n$, PTFE). This can lead to an increase of the

Table 4
EPR parameters of PPP and fluorinated poly(*p*-phenylene)

Sample	ΔH_{pp} (G)	*g*-factor	Spin density (spin g^{-1})
PPP	5.2 ± 0.2	2.0029 ± 0.0005	$1.7 \times 10^{17} \pm 0.4 \times 10^{17}$
PPPF (25 °C-5 h)	8.1 ± 0.2; 90 ± 5	2.0034 ± 0.0005	$4.4 \times 10^{19} \pm 0.9 \times 10^{19}$
PPPF (25 °C-12 h)	100 ± 5	2.0035 ± 0.0005	$4.6 \times 10^{20} \pm 0.9 \times 10^{20}$
PPPF (25 °C-24 h)	104 ± 5	2.0030 ± 0.0005	$3.3 \times 10^{20} \pm 0.7 \times 10^{20}$

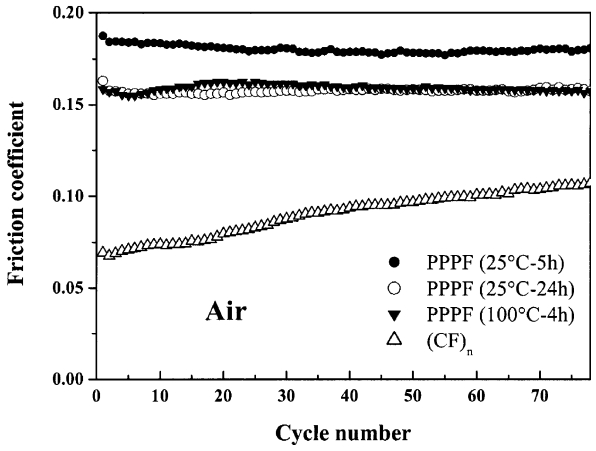

Fig. 8. Evolution of friction coefficient of fluorinated PPP and commercial $(CF)_n$ as a function of cycle number under air.

interactions between clusters or nanocrystals of PPPF in the presence of oxygen or water molecules.

Finally, the better friction results are obtained for higher fluorination temperature or longer fluorination time, i.e. fluorine content ($\mu = 0.16$ under air and $\mu = 0.13$ under argon for both PPPF (100 °C-4 h) and PPPF (25 °C-24 h)). This points out that friction properties are strongly dependent on the fluorination yield. The decrease of friction coefficient as a function of fluorine content can be related both to the lowering of surface energy and the partial ordering of the fluorinated compounds, these two parameters leading to a decrease of the energy needed to initiate sliding between microcrystals and/or PPPF molecules.

In order to confirm the role played by PPPFs crystalline structure (short length molecules, partial ordering), tribological properties of highly fluorinated PPPF have been compared to those of PTFE (long chains, amorphous). The friction coefficient obtained with PPPF compounds under air are of 0.16 whereas PTFE exhibit a friction coefficient of 0.20 [56,57]. This seems to point out that the short length and the partial ordering of PPPF molecules enhance the sliding ability of the fluorinated chains.

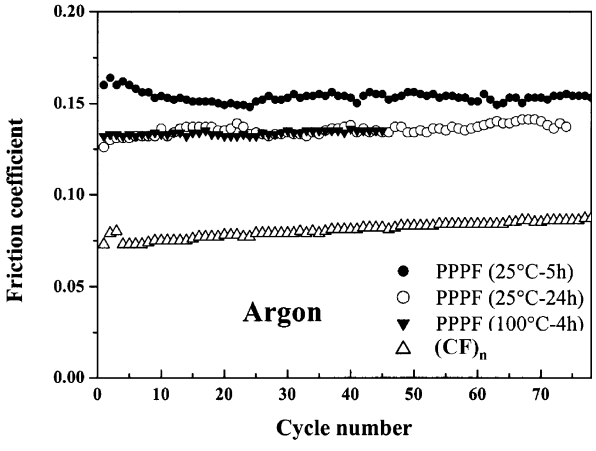

Fig. 9. Evolution of friction coefficient of fluorinated PPP and commercial $(CF)_n$ as a function of cycle number under argon.

4. Conclusion

The use of different durations and temperatures for fluorination of poly(*p*-phenylene) allows the fluorination steps to be investigated. First, the six carbon atoms cycles are partly maintained and fluorinated by conversion of C–H bonds into C–F ones forming –CF=CF–, >CHF and $>CF_2$ groups. When time and temperature of fluorination are increased, short aliphatic chains and terminal $-CF_3$ groups are created resulting from the opening of the rings. At this step, although low fluorination temperatures (25 and 100 °C), the obtained materials exhibit similarities with conventional high temperature graphite fluoride as magnified by NMR, XRD and EPR characterizations. Nevertheless, the fluorine content is higher in fluorinated poly (*p*-phenylene) than in graphite fluoride; the ratio F/C is close to 8/6 for PPPF (25 °C-24 h) whereas it is equal to one in conventional $(CF)_n$.

The study of the tribological properties of fluorinated PPP have shown the influence of experimental conditions on the friction coefficient. Moreover, PPPFs exhibit better friction performances than PTFE and can be considered as promising candidates for solid lubrication. The structure of the compounds strongly influences the tribological results which suggest that controlling crystallisation of PPPF should enhance the friction properties.

The presence of CF_3 groups is not favorable for the electrochemical performance of the fluorinated polymer since they are not electrochemically active because they require too much energy to be reduced [58]. A key point to optimize the electrochemical and tribological performance consists in the control of the fluorination processes in order to avoid the formation of such $-CF_3$ groups. This requires low duration and low temperature of fluorination and/or the use of a gaseous mixture of F_2/N_2 in order to decrease the reactivity of fluorine. Such conditions could result in more homogenous materials than those obtained in this preliminary study. Moreover, the one-dimensional character of poly(*p*-phenylene) could then allow, after fluorination, a good electrochemical lithium accessibility to the C–F sites when the fluorinated polymer is used as electrode material in lithium batteries. Electrochemical performance of fluorinated poly(*p*-phenylene) are under investigation.

References

[1] Nakajima T. Synthesis, structure, and physicochemical properties of fluorine–graphite intercalation compounds. In: Nakajima T, editor. Fluorine–carbon and fluoride–carbon materials. New York: Marcel Dekker; 1995 [chapter 1].

[2] Touhara H, Okino F. Carbon 2000;38(2):241–67.
[3] Sato Y, Shiraishi S, Mazej Z, Hagiwara R, Ito Y. Carbon 2001;41(10): 1971–7.
[4] Mickelson ET, Huffman CB, Rinzler AG, Smalley RE, Hauge RH, Margrave JL. Chem Phys Lett 1998;296(1–2):188–94.
[5] Hamwi A, Alvergnat H, Bonnamy S, Beguin F. Carbon 1997;35(6): 723–8.
[6] Touhara H, Kadono K, Watanabe N, Braconnier JJ. J Electrochem Soc 1987;134(5):1071–5.
[7] Nakajima T, Kasamatsu S, Matsuo Y. Eur J Solid State Inorg Chem 1996;33(9):831–40.
[8] Touhara H, Okino F. Fluorinated fullerenes. In: Nakajima T, Zemva B, Tressaud A, editors. Advanced inorganic fluorides: Synthesis, characterization and applications. Oxford: Elsevier; 2000 [chapter 17].
[9] Hamwi A, Latouche C, Marchand V, Dupuis J, Benoit R. J Phys Chem Solids 1996;57(6–8):991–8.
[10] Claves D, Giraudet J, Hamwi A, Benoit R. J Phys Chem B 2001; 105(9):1739–42.
[11] Ando T, Yamamoto K, Matsuzawa M, Takamatsu Y, Kawasaki S, Okino F. Diamond Relat Mater 1996;5(9):1021–5.
[12] Reisinger JJ, Hillmyer MA. Prog Polym Sci 2002;27(5):971–1005.
[13] Cihaner A, Önal AM. Eur Polym J 2001;37(9):1767–72.
[14] Kharitonov AP. J Fluorine Chem 2000;103(2):123–7.
[15] Yazami R. Electrochemical properties of graphite fluorides, metal fluorides, and oxide fluoride GICs. In: Nakajima T, editor. Fluorine–carbon and fluoride–carbon materials. New York: Marcel Dekker; 1995 [chapter 7].
[16] Nakajima T, Watanabe N. Graphite fluorides and carbon–fluorine compounds. Boca Raton: CRC Press; 1991.
[17] Fusaro RL, Sliney HE. ASLE Trans 1970;13(1):56–65.
[18] Watanabe N, Nakajima T, Touhara H. Graphite fluorides. Amsterdam: Elsevier; 1988.
[19] Dresselhaus MS, Endo M, Issi JP. Physical properties of fluorine and fluoride–graphite intercalation compounds. In: Nakajima T, editor. Fluorine–carbon and fluoride–carbon materials. New York: Marcel Dekker; 1995 [chapter 4].
[20] Hamwi A, Yazami R. Patent WO90/07798.
[21] Hamwi A. J Phys Chem Solids 1996;57(6–8):677–88.
[22] Dubois M, Guérin K, Pinheiro JP, Masin F, Fawal Z, Hamwi A. Carbon 2004;42(10):1931–40.
[23] Yamamoto T, Bundo M, Yamamoto A. Chem Lett 1977;7:833–4.
[24] Chaturvedi V, Tanaka S, Kaeriyama K. Macromolecules 1993;26(10): 2607–11.
[25] Taylor SK, Bennet SG, Khoury I, Kovacic P. J Polym Sci, Polym Lett Ed 1981;19(2):85–7.
[26] Kovacic P, Oziomek J. J Org Chem 1964;29(1):100–4.
[27] Kovacic P, Jones MB. Chem Rev 1987;87(2):357–79.
[28] Froyer G, Maurice F, Goblot JY, Fauvarque JF, Petit MA, Digua A. Mol Cryst Liq Cryst 1985;118(1–4):267–72.
[29] Mohammad F, Calvert PD, Billingham NC. J Phys D, Appl Phys 1996;29(1):195–204.
[30] Panich AM. Synth Met 1999;100(2):169–85.
[31] Miller JB, Dybowski C. Synth Met 1983;6:65–8.
[32] Barbarin F, Berthet G, Blanc JP, Fabre C, Germain JP, Hamdi M, et al. Synth Met 1983;6:53–9.
[33] Delabarre C, Guérin K, Dubois M, Giraudet J, Fawal Z, Hamwi A. J. Fluorine Chem. in press.
[34] Guérin K, Pinheiro JP, Dubois M, Fawal Z, Masin F, Yazami R. Chem Mater 2004;16(9):1786–92.
[35] Panich AM, Shames AI, Nakajima TJ. Phys Chem Solids 2001;62(5): 959–64.
[36] Panich AM, Nakajima T, Vieth HM, Privalov A, Goren SD. J Phys: Condens Matter 1998;10(34):7633–42.
[37] Panich AM, Nakajima T, Goren SD. Chem Phys Lett 1997;271(4–6): 381–4.
[38] Krawietz TR, Haw JF. Chem Commun 1998;(19):2151–2.
[39] Hagaman EW, Murray DK, Del Cul GD. Energy Fuels 1998;12(2): 399–408.
[40] Abragam A. The principles of nuclear magnetism. London: Oxford University Press; 1961.
[41] Harris RK, Monti GA, Holstein P. ^{19}F NMR. In: Ando I, Asakura T, editors. Solid state NMR of polymers, studies in physical and theoretical chemistry, vol. 84. Amsterdam: Elsevier; 1998 [chapter 18].
[42] Aeiyach S, Lacaze PC. J Polym Sci A, Polym Chem 1989;27(2): 515–26.
[43] Aeiyach S, Soubiran P, Lacaze PC, Froyer G, Pelous Y. Synth Met 1989;32(1):103–12.
[44] Lagow RJ, Margrave JL. Prog Inorg Chem 1979;26:162–210.
[45] Kharitonov AP, Kharitonova LN, Moskvin YuL, Teplyakov VV, Syrtsova DA, Koops GH, et al. Int J Plast Technol 2003;6:37–42.
[46] Kharitonov AP, Moskvin YuL, Syrtsova DA, Starov VM, Teplyakov VV. Appl Polym Sci 2004;92:6–17.
[47] Kharitonov AP, Taege R, Ferrier G, Teplyakov VV, Syrtsova DA, Koops GH. J Fluorine Chem 2005;126:251–63.
[48] Kharitonov AP, Moskvin YuL. J Fluorine Chem 1998;91:87–93.
[49] Kharitonov AP, Moskvin YuL, Teplyakov VV, Le Roux JD. J Fluorine Chem 1999;93:129–37.
[50] Ruland W. Acta Crystallogr 1961;14:1180–5.
[51] Hermans PH, Weidinger A. Macromol Chem 1961;44–46:24–36.
[52] Kovacic P, Feldman MB, Kovacic JP, Lando JB. J Appl Polym Sci 1968;12(7):1735–43.
[53] Takai K, Sato H, Enoki T, Yoshida N, Okino F, Touhara H, et al. Mol Cryst Liq Cryst 2000;340:289–94.
[54] Yokomichi H, Hayashi T, Amano T, Masuda A. J Non-Cryst Solids 1998;227–230(1):641–4.
[55] Yokomichi H, Morigaki K. J Non-Cryst Solids 2000;266–269(2): 797–802.
[56] Li F, Yan F, Yu L, Liu W. Wear 2000;237(1):33–8.
[57] Sawyer WG, Freundenberg KD, Bhimaraj P, Schadler LS. Wear 2003; 254(5–6):573–80.
[58] Hamwi A, Guérin K, Dubois M. Fluorine-intercalated graphite for lithium battery. In: Nakajima T, Groult H, editors. Fluorinated materials for energy conversion. Elsevier 2005 [chapter 17].